Spatially resolved studies of charge-density-wave dynamics and phase slip in $NbSe_3$

T. L. Adelman, M. C. de Lind van Wijngaarden, S. V. Zaitsev-Zotov,* D. DiCarlo, and R. E. Thorne

Laboratory of Atomic and Solid State Physics, Clark Hall, Cornell University, Ithaca, New York 14853-2501

(Received 30 August 1995)

We have performed spatially resolved measurements of the charge-density-wave (CDW) response to bipolar current pulses. These measurements directly yield the distribution of the CDW phase slip, the temporal evolution of the CDW elastic-force and strain profiles, and the local relationship between the phase-slip rate and strain. The steady-state elastic-force profile is strongly coupled to the phase-slip distribution. This coupling increases the CDW strain gradient near the current contacts, and reduces the size of the region in which significant phase slip occurs. Simulations of a model for CDW dynamics that includes the elastic-force–phase-slip coupling provide an excellent quantitative account of the complex spatiotemporal response. Our results imply a revised interpretation of the pulse-sign memory effect, establish the connection between CDW strains and the phase-slip voltage, provide insight into the processes underlying phase slip, and have broad implications for the understanding of previous transient and steady-state measurements in CDW systems.

I. INTRODUCTION

In quasi-one-dimensional metals such as $NbSe_3$, collective charge transport by moving charge-density waves (CDW's) results in many unusual phenomena.[1] A CDW consists of a modulation of the conduction electron density $\Delta n(x)=n_1\cos[Qx+\phi(x,t)]$ and an associated modulation of the positions of the lattice atoms. The modulation wave vector $\mathbf{Q}$ is determined by a nesting vector of the quasi-one-dimensional Fermi surface, $\mathbf{Q}=2\mathbf{k}_f$. The modulation's phase ϕ with respect to the underlying crystal lattice gives the phase of the CDW order parameter. Impurities pin the CDW relative to the lattice and produce spatial variations of ϕ. Applied electric fields greater than a threshold field depin the CDW and allow it to slide through the crystal, resulting in spatial and temporal fluctuations of ϕ and a current $i_c \propto \partial\phi/\partial t$.

Many properties of pinned and sliding CDW's have been analyzed by assuming that the bulk spatial and temporal variations of the CDW phase are described by[2–4]

$$\gamma\frac{\partial\phi}{\partial t}-K\nabla^2\phi=\left(\frac{en_c}{Q}\right)E+n_1\sum_{i=1}^{N_{\rm imp}}v_i\delta(\mathbf{x}-\mathbf{x}_i)\sin(\mathbf{Q}\cdot\mathbf{x}+\phi), \tag{1}$$

where γ is the intrinsic CDW damping, K is the elastic constant, n_c is the CDW condensate density, E is the applied field, and the rightmost term describes CDW interaction with randomly distributed impurities. Related equations have been used to describe depinning and dynamics of flux lattices in type-II superconductors, fluid invasion in porous media, and a variety of interface motion problems.[4] CDW's are thus viewed as a prototypical system for study of collective dynamics in the presence of disorder.

However, many properties of CDW systems cannot be accounted for by Eq. (1) because it neglects fluctuations of the CDW amplitude. More specifically, it neglects phase slip, in which amplitude defects (dislocations) form and grow in the CDW superlattice, so as to add or remove CDW phase fronts.[3,5–15] Phase slip is required for conversion between collective current and single-particle current at current contacts, and thus plays a central role in CDW transport.

As shown in Fig. 1, when the CDW is depinned between current contacts by an electric field applied between them, the CDW well beyond the contacts where the field is zero must remain pinned. The CDW thus compresses near one contact and stretches near the other, resulting in a macroscopic spatial variation of ϕ and a strain $\epsilon \propto \partial\phi/\partial x$.[7–10,14,16,17] This strain drives formation and growth of CDW dislocations, resulting in phase front addition at one contact and removal at the other and allowing steady CDW motion between the contacts. The net phase-slip rate is deter-

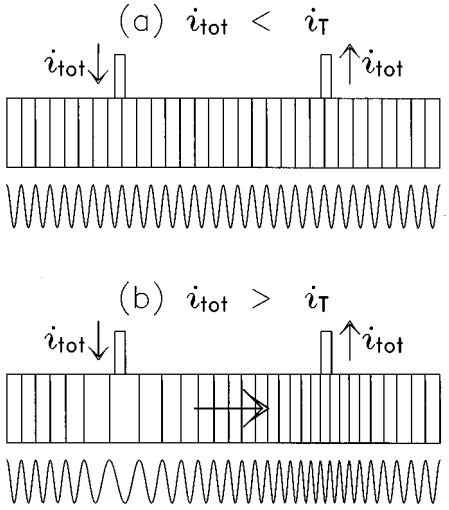

FIG. 1. A CDW crystal with two current contacts. (a) For an applied current $i_{tot}<i_T$, the CDW remains pinned to impurities and is unstrained. (b) For $i_{tot}>i_T$, the CDW between the contacts depins from impurities but the CDW well beyond the contacts remains pinned, so that the CDW becomes compressed near one contact and stretched near the other. (The CDW in $NbSe_3$ has a negative charge, and moves in a direction opposite to that indicated.)

mined by the strain profile, and determines the steady-state CDW current i_c.[9,10,14] Contact-related CDW deformations and phase slip dominate the measured properties of CDW materials at lower temperatures and in shorter samples, and are responsible for most CDW memory effects. Phase slip is also required in the temperature variation of the CDW wave vector,[18] the breakup of the CDW as it is warmed through the Peierls transition,[7,19] the depinning of inhomogeneously pinned CDW's,[20] and perhaps also in the depinning of localized regions of the CDW in large samples.[21]

Here we describe spatially resolved measurements of the CDW response to bipolar current pulses. Analysis of these measurements yields the temporal evolution of the CDW strain profile and the distribution of phase slip between the current contacts. Simulations of a model for CDW dynamics in the presence of phase slip provide an excellent account of the complex spatiotemporal response. These results provide detailed insight into the phase-slip process and its role in CDW dynamics, and have broad implications for interpretation of previous measurements. Preliminary results of this work have been reported elsewhere.[22,23]

The outline of this paper is as follows. Section II reviews previous work on contact-related CDW deformations and phase slip. Section III describes sample preparation and measurement techniques. Sections IV A and IV B present the experimental results. Analysis of these results in Sec. IV C establishes a connection between the CDW current and elastic-force profiles, and explains the origin of the CDW transient response. Section IV D shows how the CDW strain profile and its temporal evolution can be directly determined from experiment. Section IV E combines the resulting strain profile with the measured current profile to obtain the local relationship between the phase-slip rate and strain. Section V describes simulations that include phase slip in the model of Sec. IV C, and their predictions for the transient response. Implications for interpretation of previous measurements of CDW phase slip and of the CDW transient response are discussed in Sec. VI. Broader implications for understanding of CDW systems are discussed in Sec. VII.

II. REVIEW OF PREVIOUS WORK

A. Phase slip

CDW phase slip has been widely studied using dc I-V measurements.[8,9,11,12,15,24] Early experiments found that to produce steady CDW motion between current contacts, a ''phase-slip voltage'' $V_{\rm ps}$ must be applied, in addition to the voltage required to overcome bulk pinning and damping forces. $V_{\rm ps}$ has been assumed to produce the CDW strain, which drives phase slip. Since the CDW current density is determined by the net phase-slip rate, measurements of the i_c-$V_{\rm ps}$ relation yield information about the phase-slip-rate–strain relation. Using methods introduced by Gill,[8] experiments by several groups[9,11,12,15,24] on $NbSe_3$ and TaS_3 have shown that the phase-slip rate increases rapidly with increasing $V_{\rm ps}$, and that the $V_{\rm ps}$ required to obtain a given slip rate increases strongly with decreasing temperature, suggesting that phase slip is thermally activated.

Phase slip may occur both by homogeneous and by inhomogeneous (i.e., defect-assisted) processes.[3,9,7,25] Phase slip by homogeneous thermal nucleation of dislocation loops has been analyzed by Ramakrishna *et al.*,[14] using earlier ideas of Maki[5,10] and of Feinberg and Friedel.[7] Assuming that $V_{\rm ps}$ is dropped uniformly between the current contacts and that the CDW beyond the current contacts is strongly pinned and does not move, the CDW strain between the contacts is given by

$$\epsilon(x)=\frac{1}{Q}\frac{\partial\phi}{\partial x}=\frac{en_c}{Q^2K}V_{\rm ps}\left(\frac{x}{L_c}-\frac{1}{2}\right), \tag{2}$$

where L_c is the current contact separation and x is the distance measured from one of the contacts. The strain varies linearly with position and its maximum magnitude at the contacts is determined by $V_{\rm ps}$. Strain reduces the energy barrier for thermal nucleation of dislocation loops, resulting in a local nucleation rate given by

$$r_{\rm ps}(x)=r_0\exp\left[-\left(\frac{en_c}{Q}\right)\frac{V_a}{2QK\epsilon(x)}\right], \tag{3}$$

where V_a and r_0 are related to the barrier height and attempt rate for dislocation loop nucleation, respectively. The nucleation rate varies rapidly with strain, so that most of the nucleation occurs near the current contacts, where the strain is largest. Assuming that the local phase-slip rate is determined only by the local nucleation rate (and not by the subsequent growth and motion of the dislocation loops), the net phase-slip rate can be obtained by integrating Eq. (3) over the strain profile in Eq. (2) as

$$I_c=I_0\left(\frac{V_{\rm ps}}{V_a}\right)\exp\left(\frac{-V_a}{V_{\rm ps}}\right), \tag{4}$$

where $I_0\propto L_c$ and V_a increases strongly with decreasing temperature.

Equation (4) provides a good fit to the measured i_c-$V_{\rm ps}$ relations in $NbSe_3$, and V_a values obtained from fits to different samples are consistent and show roughly the predicted temperature variation.[15,24] However, the experimental magnitude of V_a is an order of magnitude smaller than predicted in Ref. 14 for nucleation of pure edge dislocation loops, suggesting that mixed loops are nucleated or that inhomogeneous nucleation is important.[24,25] Further, experimental I_0 values do not show a predicted dependence on current contact separation L_c, suggesting that the strain profile is not linear and/or that the phase-slip distribution is different than that predicted by the analysis of Ref. 14.

B. Static and transient CDW deformations

Many experiments provide indirect evidence for the boundary-condition-related CDW deformations that drive phase slip.[9,16,26–28] The single-particle resistivity in semiconducting CDW materials such as TaS_3 and $K_{0.3}MoO_3$, which strongly couples to CDW deformations, varies with position between the current contacts and with the direction of current flow.[16] The optical transmittance of $K_{0.3}MoO_3$, which depends upon the single-particle resistivity, shows a

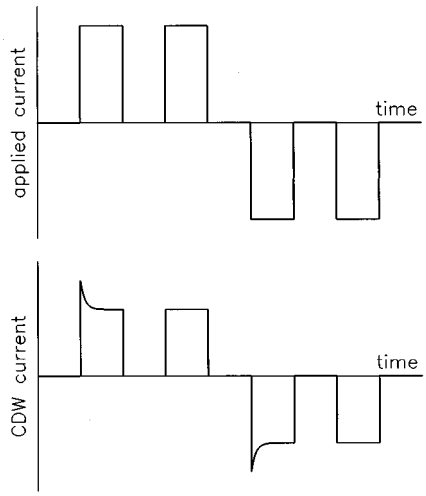

FIG. 2. The pulse-sign memory effect. When an applied current pulse is preceded by a pulse with the same sign, the CDW current follows the applied current. When the preceding pulse has opposite sign, the initial CDW current is larger than its steady-state value.

similar variation with position.[26] When the CDW is depinned in one segment of a crystal, the resulting deformations extending beyond the contacts can help or hinder depinning in an adjacent segment, depending upon the relative signs of current flow.[27]

Direct evidence for boundary-condition-related CDW deformations has been obtained from x-ray scattering measurements. Longitudinal strains produce a shift in CDW wave vector $\Delta Q(x)=\partial\phi/\partial x$. DiCarlo *et al.*[17] found that the wave-vector shift increases strongly with increasing current and decreasing temperature, similar to the measured behavior of the phase-slip voltage $V_{\rm ps}$. For the middle two-thirds of the region between current contacts probed in the experiments, the wave-vector shift varied roughly linearly with position between the current contacts, apparently consistent with Eq. (2). These results indicate a general connection between contact-related CDW deformations and $V_{\rm ps}$, and between these deformations and phase slip.

One of the most striking manifestations of phase-slip-related CDW deformations is the pulse-sign memory effect.[9,28–33] As first shown by Gill[28] and illustrated in Fig. 2, when an applied current pulse is preceded by a pulse of the same polarity, the voltage follows the current. But if the preceding pulse has opposite polarity, the initial voltage is smaller than its steady-state value, indicating that a transient excess CDW current flows. Gill suggested[9] that the transient is due to CDW motion between its steady-state strained profiles appropriate to the two current directions. X-ray scattering measurements by Sweetland *et al.*[34] showed that the time scale for the evolution of the CDW wave vector when the applied current direction is reversed is comparable to that of the transient observed in the electrical response, confirming this interpretation. However, many features of four-probe measurements of the transient response are inconsistent with simple models for the deformations.

Although previous theoretical and experimental work has illuminated many aspects of CDW deformations and phase slip, many aspects have remained obscure. First, while the analysis of Ramakrishna *et al.*[14] predicts how the local slip rate varies with strain, the effect of phase slip on the strain profile is ignored. Second, while all experiments have used side current contacts as in Fig. 1, the effect of CDW deformations (and any resulting phase slip) occuring beyond these contacts[27] on deformations and slip between them has not been accounted for. Third, while the post-nucleation growth and motion of dislocation loops has been qualitatively discussed, their effect on the rate and distribution of phase slip has not been established. Fourth, while the CDW strain and phase-slip rate are expected to vary strongly with position, the four-probe configuration used in previous dc and transient measurements effectively averages over these variations, so that the underlying local (or nonlocal) relation between slip and strain has remained obscure. And, finally, while most phase slip is expected to occur near the current contacts, neither transport measurements nor x-ray scattering measurements have probed this important region.

To address some of these issues, we have performed spatially resolved electrical measurements of the dc and transient CDW response in $NbSe_3$. These measurements provide detailed insight into the relationship between phase slip and strain in CDW conductors, and into the role of phase slip in transient CDW dynamics.

III. EXPERIMENTAL METHODS

$NbSe_3$ grows in the form of long, ribbonlike whiskers with typical thicknesses of a few micrometers, widths of a few tens of micrometers, and lengths of centimeters. Independent CDW's form below Peierls transitions at $T_{P_1}=145$ K and $T_{P_2}=59$ K.

Experiments were performed on the T_{P_1} CDW at temperatures between T_{P_1} and T_{P_2}. High-purity $NbSe_3$ single crystals were prepared using the methods described in Ref. 35. The crystals were held to alumina substrates patterned with an array of 2 μm wide, 0.25 μm high contacts, using a thin polymer film.[36] Typical contact resistances were 300 Ω, roughly two orders of magnitude larger than the sample resistance between contacts. Combined with $NbSe_3$'s electrical anisotropy, these resistances ensured that the contacts were essentially nonperturbing.

Two contact configurations were used, as shown in Fig. 3(a,b). In all measurements, the sample was current biased and the voltage response was measured for each pair of adjacent voltage contacts. The total applied current $i_{\rm tot}(t)$ flows as single-particle and CDW currents, $i_{\rm tot}(t)=i_s(x,t)+i_c(x,t)$. CDW motion, thus, reduces the single-particle current below $i_{\rm tot}$ and reduces the voltage between a given contact pair by

$$\Delta v_n=\int_{x_{n_-}}^{x_{n_+}}\rho_s i_c(x,t)\,dx, \tag{5}$$

where ρ_s is the single-particle resistivity per unit length and x_{n_-} and x_{n_+} are the positions of the voltage contacts that define the nth sample segment. The average CDW current flowing between the nth voltage contact pair is given by $i_{c_n}=\Delta v_n/R_s$. For dc measurements, Δv_n was calculated

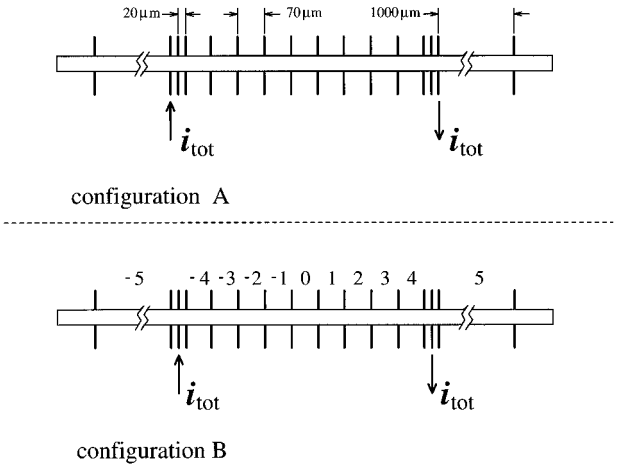

FIG. 3. Contact configurations used in the experiments. Numbers identify sample segments between adjacent voltage contacts.

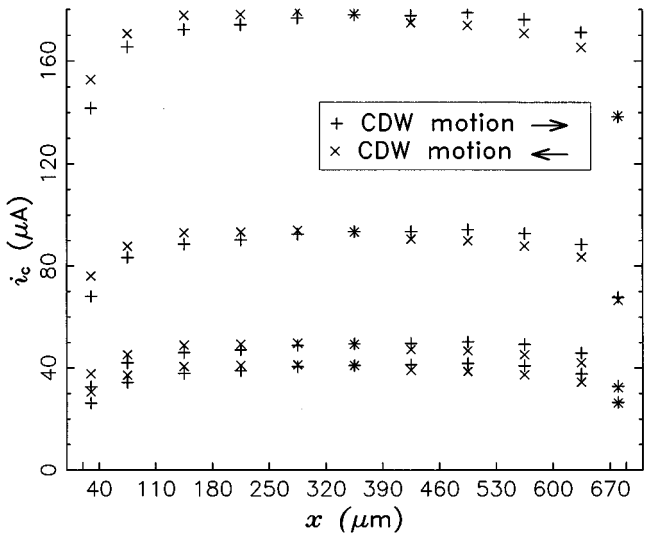

FIG. 4. Steady-state CDW current profiles in $NbSe_3$ at $T=90$ K for four different applied currents, measured using contact configuration *A* in Fig. 3. Current contacts are located at the left and right axes, and the positions of the voltage contacts are indicated on the x axis. The profiles for opposite current directions differ slightly. As shown in Fig. 9, the single-particle resistance $R_s=v/i_{tot}$ measured with $i_{tot}<i_T$ is the same for all segments and is independent of sample history, indicating that the decrease of $i_c(x)$ near the current contacts is not due to contact-geometry-related field variations or CDW deformation-related changes in R_s.

from the measured voltage v_n as $\Delta v_n=\rho_s i_{tot}-v_n$; for transient measurements, Δv_n was determined using an active bridge.

Quantitative interpretation of transient response measurements requires a careful choice of the applied current pulse sequence. An applied current pulse deforms the CDW, as shown in Fig. 1. If the current is set to zero (or reduced below threshold) at the end of the pulse, as in Fig. 2, pinning by impurities will tend to keep the CDW in this deformed state. Phase slip and CDW motion driven thermally and by the CDW elastic force will eventually relax the CDW towards an undeformed state. As a result, the magnitude of the transient observed when a current pulse of opposite polarity is applied will decrease as the pulse separation and thus the time for this relaxation is increased. The measurements were performed with zero pulse separation in order that the transient magnitude reflect the full magnitude of the CDW deformations in the two current-carrying states.

All of the experimental data presented here were measured at $T=90$ K, using a single high-purity $NbSe_3$ crystal with a thickness $t=1.9$ μm, a cross-sectional area $A=11.4$ μm^2, a threshold field $E_T(T=90\ \text{K})=160$ mV/cm, and a threshold current $I_T(T=90\ \text{K})=205$ μA. The small cross-sectional area ensured that field and current inhomogeneities due to current injection were confined to a very small region near the current contacts. Qualitatively similar behavior was observed in other samples and at other temperatures. The magnitudes of the various effects studied vary strongly with temperature.

IV. EXPERIMENTAL RESULTS AND ANALYSIS

A. Steady-state CDW current and phase-slip profiles

Figure 4 shows the CDW current in $NbSe_3$ at $T=90$ K as a function of position between current contacts, for four applied currents. The CDW current is largest in the middle of the sample and decays as the current contacts are approached. The slope of the current profile $\partial i_c/\partial x$ is proportional to the local phase-slip rate per unit length. Most of the phase slip occurs very close to the current contacts: the CDW current reaches 90% of its midsample value within 30 μm of the current contacts. Some phase slip may occur beyond the current contacts, but no current was detectable beyond 20 μm.[37] Detailed measurements of the CDW current profile as a function of current and temperature are described elsewhere.[38] Other attempts to determine this profile[39–41] have been complicated by contact perturbations.

B. Transient evolution of the CDW current profile

Figure 5 shows the transient CDW response ($\Delta v_n \propto i_{cn}$) to

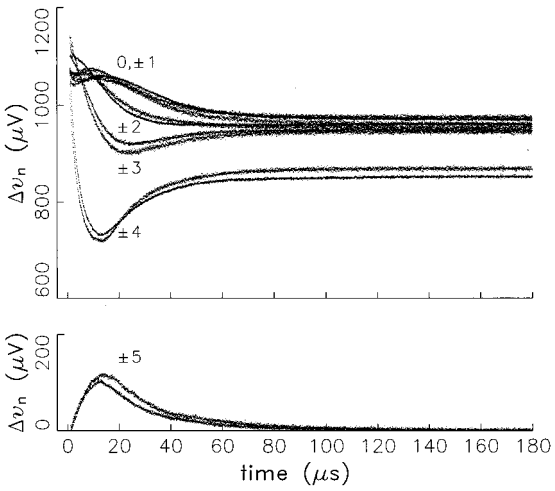

FIG. 5. CDW response in $NbSe_3$ at $T=90$ K to a sign reversal of an applied current $|i_{tot}|\approx 5i_T$, measured using contact configuration *B*. Numbers indicate the response of each sample segment in Fig. 3(b).

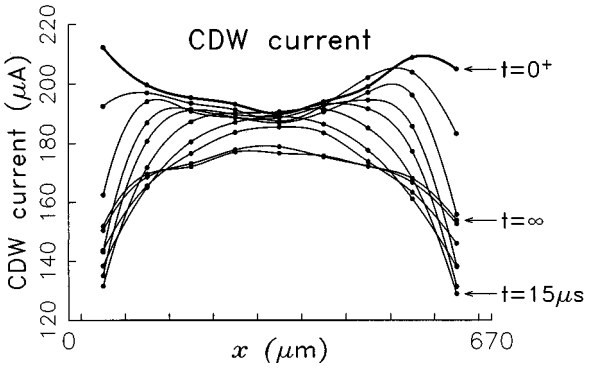

FIG. 6. Evolution of the CDW current profile when the applied current direction is reversed, calculated from the data of Fig. 5. Time $t=0^+$ indicates the profile immediately after the current direction reversal, and $t=\infty$ indicates the steady-state profile. The solid lines are guides to the eyes.

a reversal of the applied current $|i_{\rm tot}|\approx 5I_T$, for each of the sample segments indicated in Fig. 3. Figure 6 shows the corresponding transient evolution of the CDW current profile.[42] The response is roughly symmetric about the midpoint between the current contacts, and has faster initial time scales and larger transients near the current contacts. The transient response observed in previous four-probe measurements[9,28–33] decreased monotonically in time, and could be fit using exponential or stretched-exponential time dependencies. In contrast, the responses of the individual segments in Fig. 5 are nonmonotonic and nonexponential, especially near the current contacts. Transient CDW motion is also observed beyond the current contacts.[43] The long-time responses in Fig. 5 correspond to the steady-state currents in Fig. 4.

C. Origin of the transient response: The CDW current-elastic force connection

To interpret the transient response of Figs. 5 and 6 we begin by considering a simplified, one-dimensional version of Eq. (1),

$$\gamma\frac{\partial\phi}{\partial t}=\left(\frac{en_c}{Q}\right)(E-E_P)+K\frac{\partial^2\phi}{\partial x^2}. \tag{6}$$

This equation determines macroscopic variations of the CDW phase ϕ associated with boundary conditions by balancing the forces due to CDW damping ($\propto\partial\phi/\partial t$), pinning ($\propto E_P$), and elasticity [$\propto K(\partial^2\phi/\partial x^2)$] with the electric force ($\propto E$). The effects of short length-scale phase variations associated with impurity pinning are accounted for using a phenomenological pinning field E_P, taken to be a function of i_c.[44] Both E_P and the electric field E vary with i_c; i_c varies with position, but the applied current $i_{\rm tot}$ does not. Using $E=\rho_s i_s$, $i_{\rm tot}=i_c+i_s$, $i_c=A(en_c/Q)\partial\phi/\partial t$, and $\rho_c=\gamma A^{-1}(en_c/Q)^{-2}$, Eq. (6) can be simplified as

$$i_c=\frac{1}{\rho_c+\rho_s}\left[\rho_s i_{\rm tot}-E_P(i_c)+\left(\frac{en_c}{Q}\right)^{-1}K\frac{\partial^2\phi}{\partial x^2}\right], \tag{7}$$

where ρ_c is the high-field CDW resistance per unit length. This equation suggests that if $E_P(i_c)$ is known, then the profile of the CDW elastic force $\sim K[\partial^2\phi/\partial x^2(x)]$ can be determined from the measured CDW current profile $i_c(x)$.

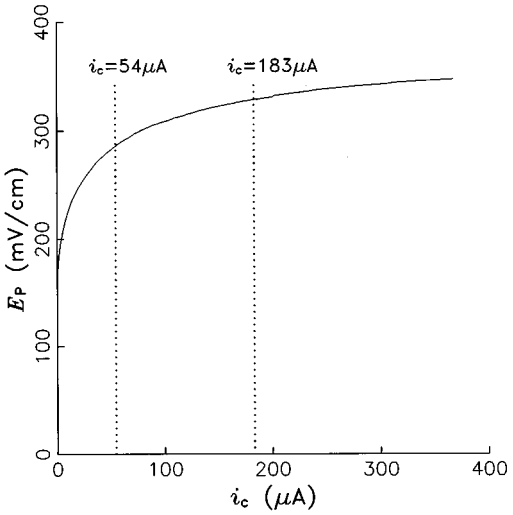

FIG. 7. Pinning field E_P at $T=90$ K for the $NbSe_3$ sample studied here. The dotted lines at 54 μA and 183 μA indicate i_c^0 for the data of Fig. 9.

$E_P(i_c)$ can be directly determined from the dc I-V relation measured using widely separated current contacts. As discussed in Sec. II, the phase-slip rate and total CDW current are determined by the CDW strain $\epsilon\propto\partial\phi/\partial x$ near the current contacts. For a given CDW current, the required strain (as indicated by the phase-slip voltage $V_{\rm ps}$) is approximately independent of current contact separation L_c.[8,9,24] Thus, for large current contact separations the elastic force $\sim K(\partial^2\phi/\partial x^2)\propto(\partial\epsilon/\partial x)\approx 2|\epsilon(x=L_c)|/L_c$ becomes very small. For L_c large compared to the voltage contact separation L_v, the CDW current will be constant between voltage contacts, because most slip occurs near the current contacts. Equation (7) then simplifies to yield

$$E_P(i_c)=\rho_s i_{\rm tot}-(\rho_c+\rho_s)i_c, \quad L_c\gg L_v. \tag{8}$$

Figure 7 shows $E_P(i_c)$ at $T=90$ K for the $NbSe_3$ sample studied here, obtained using Eq. (8) and the measured $i_c(i_{\rm tot})$ relation for $L_c\gg L_v$. When $|i_{\rm tot}|=i_T$, $E_P=E_T$. When $i_{\rm tot}\gg i_T$, E_P is nearly constant. When $|i_{\rm tot}|<i_T$, $i_c=0$, and E_P can take on a range of values between $-E_T$ and $+E_T$ to cancel the applied field E.

The relation in Fig. (7) yields the pinning force profile $E_P(x)$ for any CDW current profile $i_c(x)$. Given this relation, Eq. (7) and $i_c(x)$ thus yield the CDW elastic-force profile for any $i_c(x)>0$. For sufficiently large $i_c(x)$, such that $E_P(i_c(x))$ does not vary appreciably with position x between current contacts, the first two terms on the right-hand side of Eq. (7) are constant. Spatial variations of the elastic force will then directly follow the spatial variations of the CDW current.

Equation (7) also has implications for the transient CDW response in Figs. 5 and 6. When the current direction is suddenly reversed, measurements at $T=120$ K (where deformations due to boundary conditions are small) indicate that E_P responds with a time scale much smaller than that observed in Fig. 5. Equation (7) thus implies that the transient

variation of the elastic-force profile determines and can be determined from the transient variation of the CDW current profile. For sufficiently large $i_c(x,t)$, these transient variations directly follow each other.[45] This interconnection between the elastic force and CDW current profiles has been overlooked in previous work. It implies a revised interpretation of the transient response and, as will be discussed in subsequent sections, has broad implications for interpretation of experiments in CDW materials.

The coupling between $i_c(x,t)$ and $K(\partial^2\phi/\partial x^2(x,t)$ implied by Eq. (7) can be directly tested by comparing the steady-state and transient responses. Equation (7) can be rewritten as

$$i_c(x)=i_c^0(x)+\delta i_c(x), \tag{9}$$

where

$$i_c^0(i_{\rm tot},i_c(x))\equiv\frac{1}{\rho_c+\rho_s}[\rho_s i_{\rm tot}-E_P(i_c(x))] \tag{10}$$

and

$$\delta i_c(x)\equiv\frac{1}{\rho_c+\rho_s}\left(\frac{en_c}{Q}\right)^{-1}K\frac{\partial^2\phi}{\partial x^2}(x). \tag{11}$$

Each of these terms can be independently measured as follows:

(i) $i_c(x)$ is the steady-state CDW current profile $i_c(x,t\rightarrow\infty)$, as in Fig. 4.

(ii) $i_c^0(i_{\rm tot},i_c(x))$ is the CDW current, due to $i_{\rm tot}$ and $E_P(i_c)$ alone. Although $i_{\rm tot}$ is constant, i_c may vary with position, producing variations in $E_P(i_c)$ and thus in i_c^0. For small i_c, i_c^0 must be explicitly determined from the applied $i_{\rm tot}$ and the measured $E_P(i_c)$. For large $i_c(x)$ and i_c^0, $E_P(i_c(x))$ is roughly independent of position and equal to $E_P(i_c^0)$. i_c^0 is then roughly independent of position and equals i_c measured using widely spaced current contacts with $L_c\gg L_v$.

(iii) δi_c is the CDW current due to the CDW elastic force alone. In the steady state, the elastic force hinders CDW motion between the current contacts, so that the sign of δi_c is opposite to that of i_c^0. When the driving current $i_{\rm tot}$ changes sign, i_c^0 also changes sign and the elastic force initially aids CDW motion by an amount equal to its hindrance in the steady state. Therefore, δi_c can be determined from the transient part of the CDW current as $\delta i_c=[i_c(x,t\rightarrow\infty)-i_c(x,t=0^+)]/2$.

Equation (9) thus predicts that the dc CDW current profiles i_c and i_c^0 and the transient CDW current profile δi_c, which have no obvious *a priori* connection, should be related in a simple, quantitative way. This relation between the current profiles is illustrated schematically in Fig. 8.

Figure 9 compares measured values of i_c and $i_c^0+\delta i_c$ in $NbSe_3$ at $T=90$ K, for two applied currents $i_{\rm tot}$. For both currents, the i_c values between the current contacts are such that E_P is approximately constant.[45] The excellent agreement — with no adjustable parameters — confirms the coupling between the CDW current and elastic force. Furthermore,

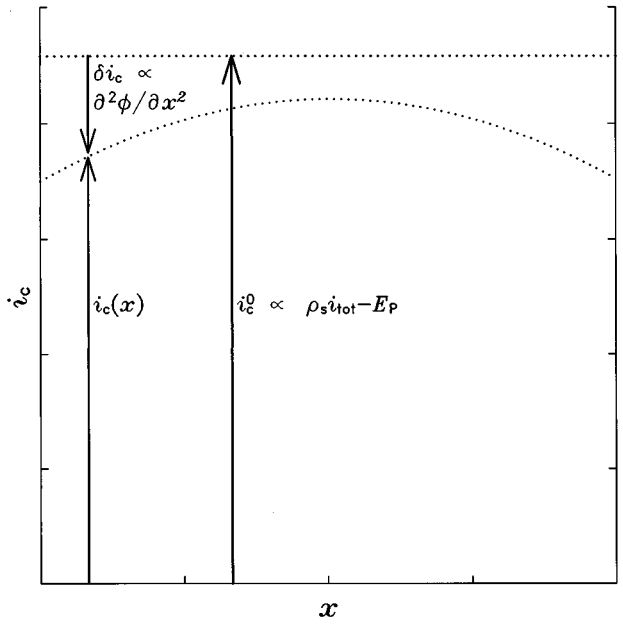

FIG. 8. Schematic illustration of the relation between the current profiles $i_c(x)$, i_c^0, and $\delta i_c(x)\propto\partial^2\phi/\partial x^2$ implied by Eq. (7). The applied force ($\propto i_{\rm tot}$) minus the pinning force ($\propto E_P$) must equal the damping force ($\propto i_c$) plus the elastic-force ($\propto\delta i_c$), so that the CDW current and elastic-force profiles must be coupled. The profiles shown are for the case of large CDW currents, for which E_P and thus i_c^0 are constant. For small CDW currents, i_c^0 will decrease near the current contacts due to the variation of $E_P(i_c)$.

Fig. 9 indicates that phase-slip-related variation of i_c near the current contacts has a dramatic effect on the elastic force in this region. For example, at 55 μm from the current contacts in Fig. 9, i_c is only 10% below its midsample value. But this

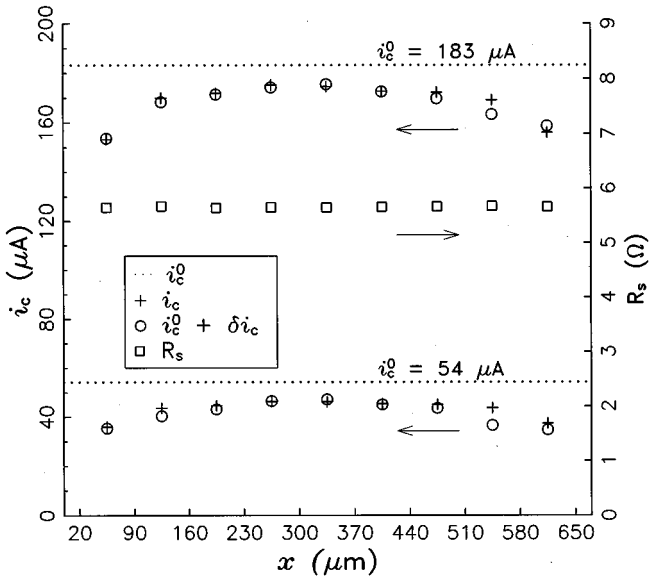

FIG. 9. Comparison of measured profiles of i_c and $i_c^0+\delta i_c$ for two applied currents. Current contacts are located at positions corresponding to the left and right vertical axes. The excellent agreement confirms the coupling between the CDW current and elastic-force profiles. The single-particle resistance $R_s=v/i_{\rm tot}$ measured with $i_{\rm tot}<i_T$ is the same for all segments and is independent of sample history.

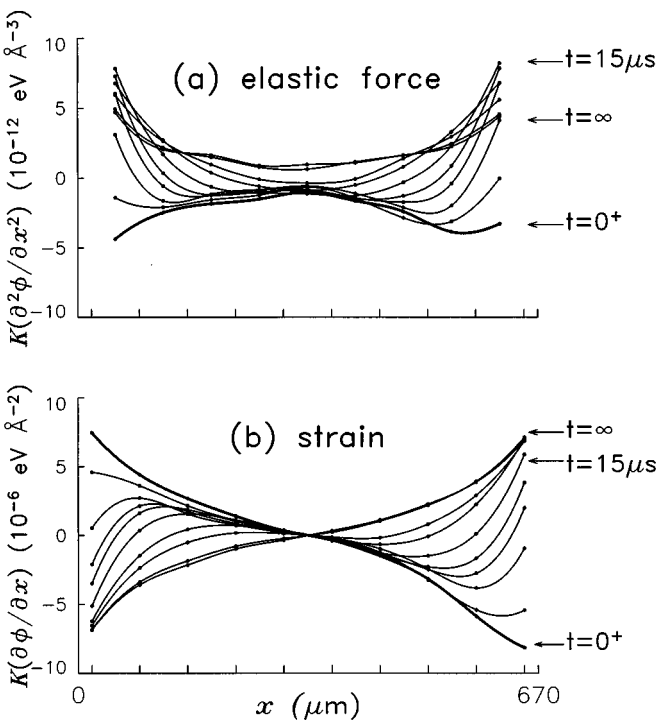

FIG. 10. Evolution of (a) the CDW elastic-force profile and (b) the CDW strain profile after a reversal in the applied current. The profiles are calculated from the transient response in Fig. 5 using Eq. (7). The dots in (a) indicate the average elastic force for each segment, and are positioned midway between adjacent voltage contacts. The dots in (b) indicate the strain at each voltage contact. The solid lines are guides to the eyes. Profiles are shown for $t=0^+$, 1, 3, 5, 10, 15, 20, 30, 50, and 60 μs.

increases the CDW elastic force (measured down from i_c^0 to i_c) by more than a factor of three.

An important assumption in the above analysis is that the single-particle resistance R_s of each sample segment is not affected by CDW deformations and phase slip. Changes in R_s would change the apparent CDW current $i_{c_n}=i_{\rm tot}-v_n/R_s$, and thus modify the measured transient and steady-state current profiles. Large changes in R_s are observed in semiconducting CDW materials, such as TaS_3 and $K_{0.3}MoO_3$, where deformation-related CDW density changes can be comparable to the equilibrium single-particle density.[1,16] But for the T_{P_1} CDW in $NbSe_3$, such changes are very small. To examine the size of deformation-related changes in R_s at $T=90$ K, the CDW was polarized by a current pulse with $|i_{\rm tol}|\gg i_T$. Changes in R_s were determined by measuring the response of each sample segment to a second pulse with $i_{\rm tot}<i_T$ using a bridge. For polarizing pulses of opposite sign, the bridge output was identical to within one one-hundredth of the overshoot size. Deformation-related changes in R_s thus have no significant effect on the CDW currents measured here.

D. The CDW Strain Profile

The analysis of the previous section provides a method for determining the CDW elastic-force profile $K[\partial^2\phi/\partial x^2(x)]$ from the CDW current profile $i_c(x)$. Figure 10(a) shows the elastic-force profile and its transient evolution for $NbSe_3$ at $T=90$ K with $|i_{\rm tot}/i_T|=5$, obtained using the $\Delta v_n(t)\propto i_{c_n}(t)$ data of Figs. 5 and 6 and the measured dc I-V characteristic i_c^0.

The CDW strain profile $\epsilon(x,t)\propto\partial\phi/\partial x$ can be obtained by integrating the elastic force $K[\partial^2\phi/\partial x^2(x,t)]$. In particular, the strain difference between adjacent voltage contacts is given by

$$\begin{aligned}\epsilon(x_{n_+},t)-\epsilon(x_{n_-},t)&=\frac{1}{Q}\int_{x_{n_-}}^{x_{n_+}}\frac{\partial^2\phi}{\partial x^2}(x,t)dx\\&=(\rho_s+\rho_c)\left(\frac{en_c}{KQ^2}\right)\int_{x_{n_-}}^{x_{n_+}}\delta i_c dx\\&=\frac{\rho_s+\rho_c}{\rho_s}\left(\frac{en_c}{KQ^2}\right)[\Delta v_n\\&\quad-(x_{n_+}-x_{n_-})\rho_s i_c^0],\end{aligned}\tag{12}$$

where x_{n_-} and x_{n_+} are the positions of the two contacts that bound the nth sample segment and Δv_n is the response of that segment. Note that this equation gives the exact strain difference between the voltage contacts, and not a space-averaged value. These strain differences determine the strain profile to within an unknown offset ϵ_0. Previous work has shown that the phase-slip rate depends upon the CDW strain. Equation (12) shows that the CDW strain depends upon the CDW current distribution, and thus upon the distribution of phase slip.

Figure 10(b) shows the time evolution of the strain profile calculated using Eq. (12) and the data of Fig. 5, with ϵ_0 chosen for each profile so that the strain in the center of the sample is zero.[46] Near the sample center, where the CDW current is approximately constant, the steady-state strain varies approximately linearly with position, consistent with previous x-ray measurements.[17] Near the current contacts, where phase slip produces a smaller CDW current, the steady-state strain is significantly enhanced over its linear extrapolation. Furthermore, the strain's transient evolution near the current contacts is much more rapid than near the sample center. For example, after 15 μs the strain 20 μm from the current contacts has advanced to 90% of its final value, while the strain 140 μm from the current contacts has advanced to only 30% of its final value. Recent spatially resolved measurements by Itkis and Brill[47] of the optical transmittance of $K_{0.3}MoO_3$ — which couples to the CDW strain — have yielded steady-state profiles that are qualitatively similar to that in Fig. 10(b).

E. The local slip-strain relation

Previous four-probe measurements of $i_c-V_{\rm ps}$ relations show how the total phase-slip rate varies with the average strain magnitude within a sample. The present measurements of the CDW current profile yield both the phase-slip profile $r_{\rm ps}(x)\propto\partial i_c/\partial x$ and the strain profile $\epsilon(x)$. Comparison of these profiles thus gives a direct estimate of the *local* relationship between the phase-slip rate and strain, $r_{\rm ps}(\epsilon(x))$.

The strain at each voltage contact between the current contacts is determined from the CDW current profile in Fig.

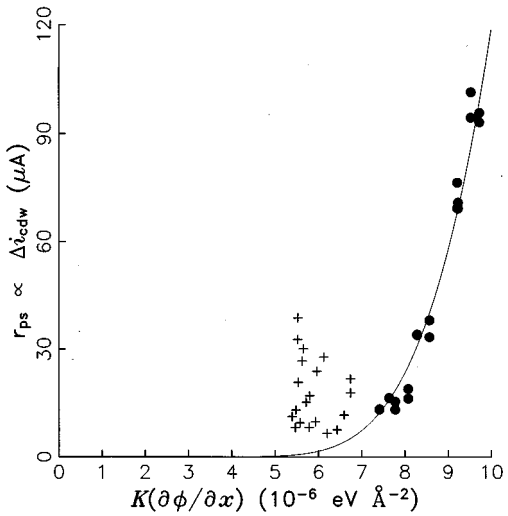

FIG. 11. Local phase-slip rate versus local strain at two positions, determined using contact configuration *B*. (●) indicates estimated values at the current contacts. (+) indicates values 40 μm from the current contacts. The solid line is a fit of the current contact data to Eq. (3).

4 using Eq. (12), with $i_c^0(i_{\rm tot}, i_c)$ determined from the measured $E_P(i_c)$ relationship. The phase-slip rate per unit length at each voltage contact can be estimated from the difference between CDW currents measured for sample segments on either side of it.

Most phase slip occurs very near to the current contacts. The strain at each current contact can be estimated by extrapolating the strains at the two nearest voltage contacts, 20 μm and 40 μm away.[48] The phase-slip rate at each current contact can be estimated from the CDW current measured between the nearest voltage contact pair. This CDW current is created or destroyed by phase slip occurring between these contacts, between the current contact and these contacts, and beyond the current contact. Most of this phase slip occurs in the immediate vicinity of the current contact, and simulations discussed in Sec. V suggest that phase slip is distributed roughly symmetrically about the contact. Thus, the phase-slip rate at each current contact is estimated from half the CDW current measured between the nearest voltage contact pair.

Figure 11 shows the resulting $r_{\rm ps}(\epsilon)$ relations at a current contact and at a voltage contact 75 μm from the current contact. The solid line indicates a fit of the current contact data to the local slip-rate–strain relation Eq. (3) predicted in Ref. 14. The value $V_a = 31$ mV obtained from this fit is close to the value $V_a = 35$ mV obtained from fits to four-probe measurements by Maher *et al.*[15,24] for $NbSe_3$ at $T = 90$ K. The fit value $r_0 \approx 5\times10^{15}$ s^{-1} m^{-1} is slightly larger than the corresponding value obtained by Maher *et al.*

Although experimental uncertainties in the $r_{\rm ps}(\epsilon)$ data at the voltage contact are large, the phase-slip rate observed there is clearly much larger for a given strain than is observed near the current contacts. This indicates that the phase-slip rate is not simply a function of strain. As discussed in Sec. VII, the position dependence of $r_{\rm ps}(\epsilon)$ suggests that the phase-slip process is nonlocal, perhaps as a consequence of dislocation motion.

V. SIMULATIONS OF TRANSIENT CDW DYNAMICS

A. Model and simulation method

The results of the previous section establish that the CDW elastic force and strain profiles are strongly coupled to the CDW current and phase-slip profiles. To gain further insight into the experimental results, we have performed numerical simulations that solve for CDW motion in the presence of phase slip. The simulation is based upon Eqs. (7) and (3) and proceeds in alternate time steps: phase is added according to Eq. (3), and the resulting phase profile then evolves according to Eq. (7). The CDW current is given by $i_c = A(en_c/Q)(\partial\phi/\partial t)$, and modifies the single-particle current $i_s = i_{\rm tot} - i_c$ and thus the electric field $E = \rho_s i_s$. This current is associated only with the post-slip phase evolution, and not with phase slip itself. The phase and current profiles evolve until, in the steady state, phase is added by phase slip at the same rate as it is removed by CDW motion and current flow.

Taken together, these time steps solve for the evolution of a phase $\theta(x,t)$, which is renumbered by phase slip and obeys

$$\frac{\partial\theta}{\partial t} = \left(\frac{Aen_c}{Q}\right)^{-1} \frac{1}{\rho_c+\rho_s}\left[\rho_s i_{\rm tot} - E_P + \left(\frac{en_c}{Q}\right)^{-1} K\frac{\partial^2\theta}{\partial x^2}\right] - \int_{-\infty}^{x} r_{\rm ps}(\theta(x',t))dx'. \tag{13}$$

The first term on the right-hand side corresponds to the dynamical evolution of the phase according to Eq. (7), and gives the CDW current ($\propto \partial\phi/\partial t$). The second term on the right-hand side accounts for phase slip. The renumbered phase θ describes spatial deformations of the CDW and remains well defined during phase slip. The original phase variable $\phi(x,t)$ does not remain well defined. For example, when a constant CDW current flows between current contacts, $\partial\phi/\partial t$ must be finite there. But well beyond the contacts, the current and thus $\partial\phi/\partial t$ must be zero. The contrast between these regions implies that ϕ is poorly defined at the boundary.

The effects of phase slip on $\theta(x,t)$ in the steady state is shown schematically in Fig. 12. Initially, the CDW is distorted. Phase slip occurs at both sides of the sample, reducing the strain near the current contacts and renumbering the phase downward between the contacts; this renumbering does not produce a CDW current. The forces acting on the CDW drive it back towards its original profile, and this motion produces a current. In this way, the phase ϕ continually advances, but θ maintains a uniform profile. Steady state in Eq. (13) is determined by $\partial\theta/\partial t = 0$.

B. Transient response simulation results

Figure 13 shows the voltage response $\Delta v_n \propto i_{c_n}$ calculated using Eq. 13 for an applied current $i_{\rm tot}$ and contact spacings equal to those used in Fig. 5. The values of the parameters $E_P(i_c)$, ρ_s, and ρ_c used in the simulation were all independently determined from steady-state measurements described earlier.[49] V_a and r_0 were obtained from the fit in Fig. 11 to the local slip–strain relation near the current contacts. The sole remaining parameter — the elastic constant K — deter-

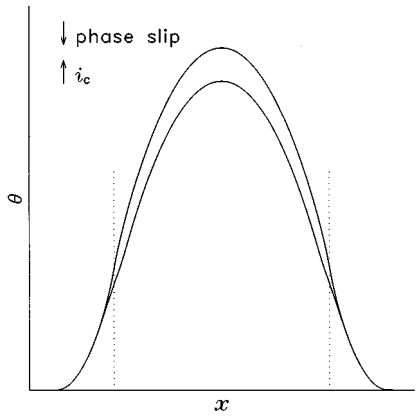

FIG. 12. Schematic illustration of a time step used in the simulation. Phase slip occurs near the current contacts (indicated by dotted vertical lines), reducing the CDW strain there and shifting the CDW phase θ between the contacts downward. CDW motion, driven by the applied current, increases θ between the contacts and the strain near the contacts. In the steady state, the phase change per unit time due to phase slip is equal in magnitude to that due to CDW motion and $(\partial\theta/\partial t)(x,t)=0$.

mines the time scale of the response. A value $K=6.2\times10^{-3}$ eV Å^{-1} produced the correct time scale, and is consistent with the value reported by DiCarlo *et al.*[17,50] The calculated response reproduces most of the important qualitative and quantitative features seen in Fig. 5. This excellent agreement provides confidence in the model and simulation, and justifies their use to study underlying aspects of transient CDW dynamics that are not readily accessible in experiments.

Figure 14 shows the corresponding simulation results for the evolution of the CDW phase, strain, elastic force, phase slip, and current profiles. The heavy lines indicate the steady-state profiles appropriate to the initial current direction; except for the current, the final profiles are symmetric to these.

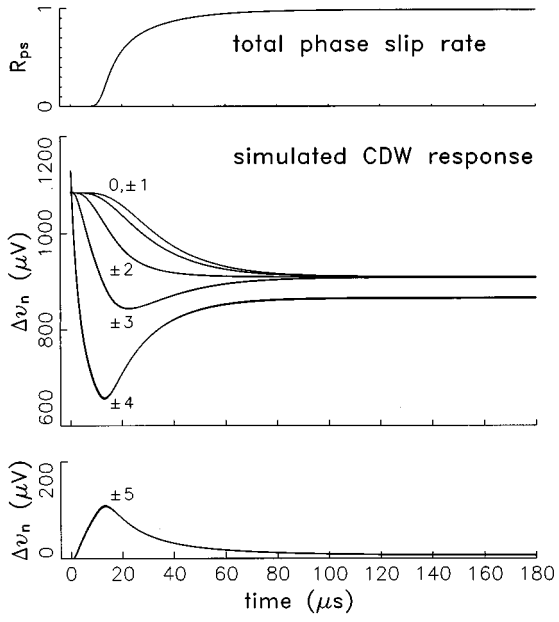

FIG. 13. CDW response to a sign reversal of the applied current calculated using Eq. (7) for the conditions and contact configuration in Fig. 5. $R_{ps}(t)$ is the total phase-slip rate $\int_{-\infty}^{+\infty}|r_{ps}|dx$ normalized by its steady-state value.

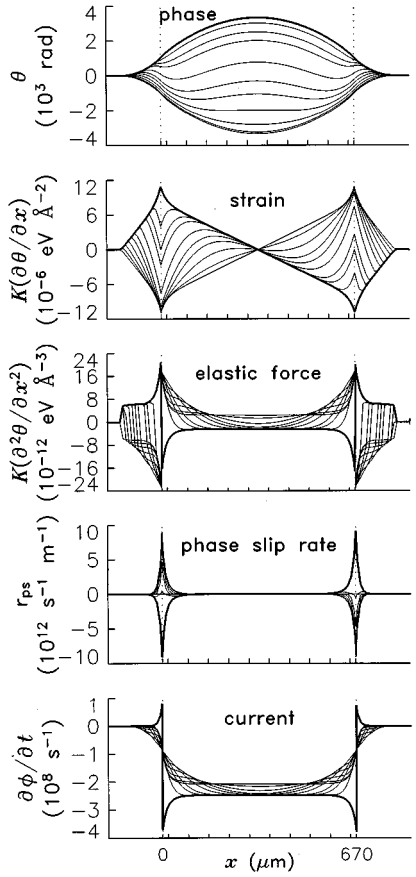

FIG. 14. Simulated evolution of the CDW phase, strain, elastic force, phase slip, and current profiles, corresponding to the simulated and measured transient responses in Figs. 13 and 5. Current contacts are located at $x=0$ and 670 μm, indicated by the dotted vertical lines. Profiles are shown for $t=0^+$, 1, 3, 5, 10, 15, 20, 30, 50, 60, 100, 300 μs. Heavy lines indicate $t=0^+$.

The steady-state CDW phase in Fig. 14(a) has a roughly parabolic profile between the current contacts and decays to zero at a distance of roughly 100 μm beyond the current contacts. When the current direction is reversed, the parabolic profile between the current contacts tries to move downward uniformly, but elastic interaction with the pinned CDW beyond the current contacts constrains this motion. This constraint is first felt near the current contacts and produces a rapid change in CDW strain and elastic force there; near the middle of the sample, this constraint affects the phase much later. The steady-state current in Fig. 14(e) decreases from its midsample maximum as the current contacts are approached. Although CDW strain extends significantly beyond the current contacts, the strain is too small to cause appreciable phase slip and the CDW current rapidly falls to zero. The elastic force in Fig. 14(c) increases where the CDW current decreases just inside the current contacts, consistent with the coupling indicated by Eq. (7). The CDW strain profile in Fig. 14(b) can be directly compared with the experimentally determined profile in Fig. 10(b).

These simulation results provide insight into the complex spatiotemporal response observed in the data of Figs. 5 and 13. Just before the applied current changes sign, the elastic force opposing CDW motion is largest near the current contacts (segments ± 4), where phase slip produces a smaller steady-state CDW current. Just after the sign change, the elastic force aids CDW motion, and thus drives a larger transient CDW current (proportional to Δv_n in Fig. 5) near the current contacts. This motion is quickly held back by the section of the CDW beyond the current contacts (segments ± 5), leading to a rapid decay of the CDW current and to an increase in strain near the contacts. As the strain near the contacts builds, it eventually becomes large enough to induce significant phase slip. Phase slip increases the CDW current from its minimum at the ''dip'' towards a larger steady-state value, and limits subsequent growth of the strain near the contacts. Since CDW motion beyond the current contacts (segments ± 5) is only driven by this strain, the dips observed just inside the current contacts (segments ± 4) nearly coincide with the peaks observed just outside (segments ± 5). Near the middle of the sample (segments 0, ± 1), the CDW moves independent of the region beyond the contacts for a longer time, producing a slower transient. The response here is monotonic, since phase slip is already occuring by the time the middle region's elastic force changes sign.

The most significant discrepancy between the simulations and experiment is in the distribution of phase slip. In the simulations, essentially no slip occurs between the current contacts at distances greater than 90 μm from the contacts, whereas in the experiment roughly 4% of the slip occurs there. This discrepancy occurs because the simulation assumes a unique relation between the local slip rate and strain given by Eq. (3), contrary to the experimental results in Fig. 11.

A second discrepancy between the simulations and experiment occurs in the first 10 μs of the transient for segments 0 and ± 1, near the middle of the sample. The simulation shows a completely flat response, as expected since the effects of the boundary have not reached the middle of the sample at these early times. In contrast, the measured response $\delta v_n \propto i_{c_n}$ in Fig. 5 shows a small, sharp drop followed by a slower increase before decreasing towards its steady-state value. This behavior may be due to some detail of the bulk dynamics, such as variations in CDW pinning, as the CDW reorganizes between states of opposite motion.[51] The increase in CDW current may arise from CDW phase slip in this region, which is much larger than predicted by the simulation. For a constant applied current, strains near each current contact drive formation and growth of CDW dislocations of opposite type, and motion of the dislocations toward the center of the sample. This process removes CDW phase fronts near one contact and adds them at the other, allowing steady CDW motion between them. When the applied current direction is abruptly reversed, the strain profile away from the current contacts remains essentially unchanged for a significant time, as shown in Figs. 10(b) and 14(b). Dislocations present just before the current direction reversal (of opposite sign to those appropriate to the new direction) thus will continue to grow and remove phase fronts, allowing the CDW strain to relax without moving the CDW. As a result, the transient CDW current will be smaller than that for purely elastic strain relaxation. Once these dislocations have been removed, the subsequent evolution of the CDW phase will be elastic until the strains near the contacts again become large enough to generate dislocations. Since the simulations assume a local slip-rate–strain relation as determined near the current contacts, they underestimate slip away from the contacts and ignore slip due to growth in low-strain regions of dislocations formed in high-strain regions. These ideas suggests that transient response measurements may be useful in studying CDW dislocation dynamics.

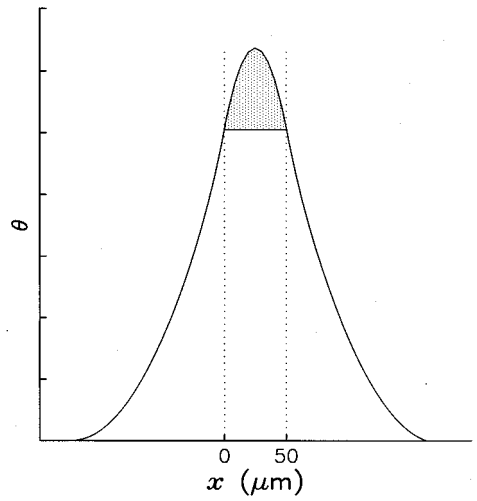

FIG. 15. Simulated phase displacement profile for $i_c \approx 50$ μA, calculated using a 50 μm current contact separation and other parameters as in Fig. 13. Roughly 80% of the midsample phase displacement is due to CDW deformations beyond the current contacts.

C. CDW deformations beyond current contacts

The remarkably large transient response observed beyond the current contacts in the data of Fig. 5 shows that substantial CDW displacements occur in this region. Although the magnitude of these displacements cannot be determined from the data, the close agreement between the measured and simulated responses for segments ± 5 gives some confidence that the simulation correctly predicts the behavior beyond the contacts. We have thus used the simulations to investigate this behavior and its effects on the CDW response between the contacts.

Figure 15 shows the phase profile for $i_c \approx 50$ μA, calculated using a 50 μm current contact separation and other parameters as described in Sec. V B. 80% of the midsample phase displacement in this short segment is due to CDW deformations beyond the current contacts; deformations between the contacts account for only 20%. Displacements beyond the current contacts thus dominate the total phase displacement in sufficiently short samples. Beyond the current contacts, i_c is very small, so that the elastic force is balanced only by the pinning force. Consequently, the extent of the deformed region beyond the contacts and its contribution to the total phase displacement decreases with increasing pinning strength and E_T.

Two quantities are useful for characterizing the phase displacement: the midsample phase displacement θ_{peak}, and the space-averaged displacement

TABLE I. Comparison of the maximum CDW phase displacement θ_{peak} and the space-averaged phase displacement $\bar{\theta}$ obtained from simulations using three different inner contact pair separations. The values are for applied currents i_{tot} that yield the same strain at the current contacts for each contact separation.

Length (μm)	θ_{peak}	$\bar{\theta}$
50	1020	2310
140	1340	1660
670	2920	2340
3000	8470	6030

$$\bar{\theta}=\frac{1}{L}\int_{-\infty}^{+\infty}\theta(x)dx. \tag{14}$$

Note that both θ_{peak} and $\bar{\theta}$ use the renumbered phase θ rather than ϕ (as discussed in Sec. V A), so as to meaningfully characterize CDW displacements in the presence of phase slip.

Table I gives values of θ_{peak} and $\bar{\theta}$ calculated from steady-state profiles for current contact separations L_c of 50, 140, 670, and 3000 μm. The applied current i_{tot} was set independently for each L_c to yield the same strain at the current contacts; this is analogous to typical experimental comparisons, which are made for the same V_{ps}. According to Eq. (2) of Ramakrishna *et al.*, which neglects CDW motion beyond the current contacts and the CDW current–elastic-force coupling, the CDW phase displacement profile should be parabolic, and for fixed V_{ps}, both θ_{peak} and $\bar{\theta}$ should vary linearly with L_c. θ_{peak} and $\bar{\theta}$ in Table I generally do increase with L_c, but the increase is far from linear: θ_{peak} and $\bar{\theta}$ increase by factors of roughly 9 and 3, respectively, for a factor of 60 increase in L_c; $\bar{\theta}$ even decreases slightly as L_c increases from 50 to 140 μm. Even for $L_c=670$ μm, used in the experiments of Sec. IV B and the simulation of Fig. 14, almost half of the midsample phase displacement is due to deformations beyond the current contacts. As will be discussed in Sec. VI C, these deformations have significant quantitative effects on the measured transient response.

VI. COMMENTS ON PREVIOUS STUDIES OF CDW DEFORMATIONS AND PHASE SLIP

The experiments and analysis presented here provide detailed insight into CDW deformations, phase slip, and the transient response in $NbSe_3$. As we will now discuss, these results have important implications for interpretation of many previous experiments.

A. DC measurements of phase slip

Many studies of CDW phase slip have employed four-probe *I-V* measurements, using a method introduced by Gill.[8,9] In the usual four-probe configuration, referred to as the normal configuration, the current is injected between the outer contact pair, separated by a distance L_{out}; the voltage is measured across the inner pair, separated by L_{in}. In the transposed configuration, the current is injected between the inner pair, and the voltage is measured across the outer pair. The average CDW current flowing between the inner contact pair is determined as

$$i_{c,norm}=i_{tot,norm}-(V_{norm}/R_s) \tag{15}$$

in the normal configuration and

$$i_{c,trans}=i_{tot,trans}-(V_{trans}/R_s) \tag{16}$$

in the transposed configuration, where $i_{tot,norm}$ and $i_{tot,trans}$ are the applied currents, V_{norm} and V_{trans} are the measured voltages, and R_s is the single-particle resistance of the segment defined by the inner contact pair. Gill showed that for equal CDW currents $i_{c,trans}=i_{c,norm}$, the voltage measured in the transposed configuration is larger than in the normal configuration, i.e.,

$$V_{tn}(i_c)\equiv V_{trans}(i_{c,\,trans}=i_c)-V_{norm}(i_{c,norm}=i_c)>0. \tag{17}$$

Gill suggested that this extra voltage drives the CDW deformations between current contacts required for phase slip. If the CDW current is assumed to be constant between the current contacts and if the extra voltage is dropped uniformly between them, the CDW strain profile is linear and the strain at the current contacts is simply proportional to V_{tn}, as in Eq. (2). Measurements of i_c as a function of V_{tn} then provide direct information about the variation of the slip rate with CDW strain. However, the present measurements show that the CDW current is not constant, that the CDW strain does not vary linearly between the current contacts, and that the current and strain are strongly coupled. How then do the measured voltages V_{trans} and V_{norm} relate to the strains which drive phase slip?

To answer this question, the quantities of interest must be defined. First, we define the phase-slip voltage $V_{ps}(i_c)$ to be the experimental voltage difference $V_{tn}(i_c)$ measured when the outer contact pair separation L_{out} is large compared with the inner contact pair separation L_{in}. In general, the measured $V_{tn}(i_c)$ depends upon the contact pair separations.[24] But for $L_{out}\gg L_{in}$, the strain-related voltage drop between current contacts makes a negligible contribution to V_{norm}, so that the measured V_{tn} is essentially independent of L_{out} and L_{in}. This definition of V_{ps} differs slightly from previous definitions,[9,11–13,15,24] but is the most meaningful. Second, we define a voltage V_{strain} for the transposed configuration as

$$V_{strain}\equiv\frac{Q}{en_c}\int_{-L_{in}/2}^{L_{in}/2}K\frac{\partial^2\theta}{\partial x^2}dx. \tag{18}$$

The integral is proportional to the difference in CDW strain between the two (inner) current contacts, or to twice the strain at one contact.[52] V_{strain} thus provides a meaningful measure of the strain that drives phase slip. In analyzing their data, Maher *et al.*[15] and DiCarlo *et al.*[17] effectively assumed that $V_{ps}=V_{strain}$. The actual relation between these quantities can be determined as follows.

Using Eqs. (15) and (16), $V_{ps}(i_c)$ can be expressed in terms of the applied currents $i_{tot,\,trans}$ and $i_{tot,norm}$ required to produce a given $i_c=i_{c,norm}=i_{c,trans}$ as

$$V_{ps}=R_s(i_{tot,trans}-i_{tot,norm}). \tag{19}$$

$i_{\mathrm{tot,norm}}$ and $i_{\mathrm{tot,trans}}$ can each be determined using Eq. (7). In the normal contact configuration, $\partial^2\theta/\partial x^2=0$, and i_c and thus $E_P(i_c)$ are constant between the inner (voltage) contact pair. Equation (7) gives

$$i_{c,\mathrm{norm}}=\frac{1}{\rho_c+\rho_s}[\rho_s i_{\mathrm{tot,norm}}-E_{P,\mathrm{norm}}]. \tag{20}$$

In the transposed configuration, the current i_c varies with position between the inner (current) contact pair. The voltage measured in this case is

$$V_{\mathrm{trans}}=\int_{-\infty}^{+\infty}\rho_s i_s(x)dx=R_s i_{\mathrm{tot,norm}}-\int_{-\infty}^{+\infty}\rho_s i_c(x)dx, \tag{21}$$

so that the current $i_{c,\mathrm{trans}}$ determined using Eq. (16) is given by

$$i_{c,\mathrm{trans}}=\frac{1}{L_{\mathrm{in}}}\int_{-\infty}^{+\infty}i_c(x)dx. \tag{22}$$

Since $\int_{-\infty}^{+\infty}(\partial^2\theta/\partial x^2)dx=[\partial\theta/\partial x(+\infty)]-[\partial\theta/\partial x(-\infty)]=0$, Eq. (7) gives

$$i_{c,\mathrm{trans}}=\frac{1}{\rho_c+\rho_s}\frac{1}{L_{\mathrm{in}}}\left[\rho_s i_{\mathrm{tot,norm}}-\int_{-\infty}^{+\infty}E_{P,\mathrm{trans}}(x)dx\right]. \tag{23}$$

Substituting for $i_{\mathrm{tot,norm}}$ and $i_{\mathrm{tot,trans}}$ from Eqs. (20) and (23), Eq. (19) becomes

$$V_{\mathrm{ps}}=-L_{\mathrm{in}}E_{P,\mathrm{norm}}+\int_{-\infty}^{+\infty}E_{P,\mathrm{trans}}(x)dx \tag{24}$$

at values of $i_{\mathrm{tot,norm}}$ and $i_{\mathrm{tot,\,trans}}$ such that $i_{c,\mathrm{trans}}=i_{c,\mathrm{norm}}$.

Equation (24) provides a general expression for V_{ps}, independent of the phase-slip mechanism and profile. Between the inner contact pair, $E_{P,\mathrm{norm}}$ and $E_{P,\mathrm{trans}}$ differ because of the nonuniform transposed current profile, but this difference is usually small. Assuming $E_{P,\mathrm{trans}}(x)=E_{P,\mathrm{norm}}$ between the inner contact pair, Eq. (24) simplifies to

$$V_{\mathrm{ps}}=\int_{\mathrm{out}}E_{P,\mathrm{trans}}(x)dx \tag{25}$$

$$=\int_{\mathrm{out}}\left[(\rho_c+\rho_s)i_{c,\mathrm{trans}}(x)-\left(\frac{en_c}{Q}\right)^{-1}\frac{\partial^2\theta}{\partial x^2}\right]dx \tag{26}$$

$$=\int_{\mathrm{out}}(\rho_c+\rho_s)i_{c,\mathrm{trans}}(x)dx+V_{\mathrm{strain}}, \tag{27}$$

where the integrals are taken over the region exterior to the inner contact pair. Since $i_{c,\mathrm{trans}}$ and $\partial^2\theta/\partial x^2$ have the same sign in this region, $V_{\mathrm{ps}}<V_{\mathrm{strain}}$. Thus, the measured V_{ps} underestimates the strain near the current contacts. The difference between V_{ps} and V_{strain} — $\int_{\mathrm{out}}(\rho_c+\rho_s)i_{c,\mathrm{trans}}dx$ — is small for small CDW currents and increases with increasing current.

To further investigate the connection between the measured i_c-V_{ps} relations and the underlying slip-rate–strain relation, we have performed simulations using the model and parameters of Sec. V. Figure 16 shows the CDW current $i_c=i_{c,\,\mathrm{norm}}=i_{c,\mathrm{trans}}$ versus both V_{ps} and V_{strain} calculated using an inner contact pair separation of 140 μm, comparable to that used in previous i_c-V_{ps} measurements. At small currents, the simulation shows little current flow beyond the current contacts, and V_{strain} and V_{ps} are nearly equal. As the current increases, more current flow is observed beyond the contacts, and V_{strain} becomes larger than V_{ps}, consistent with Eq. (27). Consequently, i_c rises faster with V_{ps} than with V_{strain}.

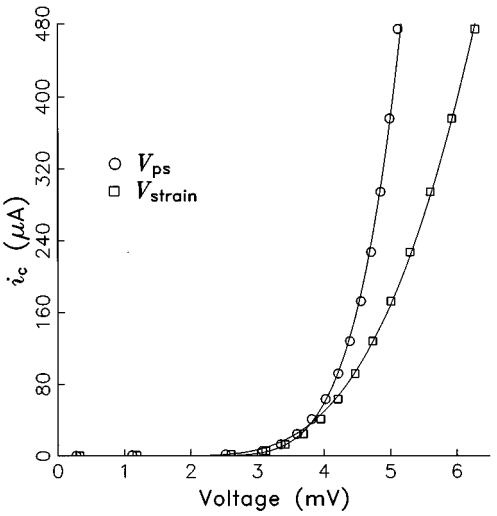

FIG. 16. Comparison of simulated i_c-V_{ps} and i_c-V_{strain} relations for a current contact separation of 670 μm and other parameters as in Fig. 13. The solid lines indicate fits to Eq. (4).

The solid lines in Fig. 16 indicate fits to the functional form Eq. (4) predicted by Ramakrishna *et al.*,[14] which provides a good fit to the measured i_c-V_{ps} relations in $NbSe_3$. This form describes the simulated i_c-V_{ps} and i_c-V_{strain} relations very well, with V_a values of 37 mV and 25 mV, respectively. These are larger and smaller, respectively, than $V_a=31$ mV used in the simulations. The predicted form Eq. (4) assumes that the CDW strain profile is linear between the current contacts and that there is no CDW current flow beyond the contacts. Since coupling between the current and phase-slip profiles enhances the strain near the contacts, appreciable phase slip occurs in a smaller region than if the strain profile were linear, so that the total phase-slip rate and current for a given contact strain and V_{strain} are reduced. This effect increases with increasing current, and thus reduces V_a obtained from the i_c-V_{strain} relation. In the i_c-V_{ps} relation, this effect is overwhelmed by a reduction in V_{ps} with increasing i_c, due to increased CDW current flow beyond the current contacts; this leads to a larger value of V_a. Despite these effects, the results of Fig. 16 indicate that the measured V_{ps} does provide a reasonable estimate of the strain at the current contacts, and that the measured i_c-V_{ps} relations yield V_a values that are comparable to those for the underlying slip-strain relation.

The strain and slip-rate enhancements near the current contacts produced by the CDW current–elastic-force coupling explain a previously puzzling discrepancy between the i_c-V_{ps} measurements of Maher *et al.*[15,24] and the predictions of Ramakrishna *et al.*[14] Assuming a linear strain profile between current contacts, the net slip rate and thus the CDW current for a given contact strain should scale with the con-

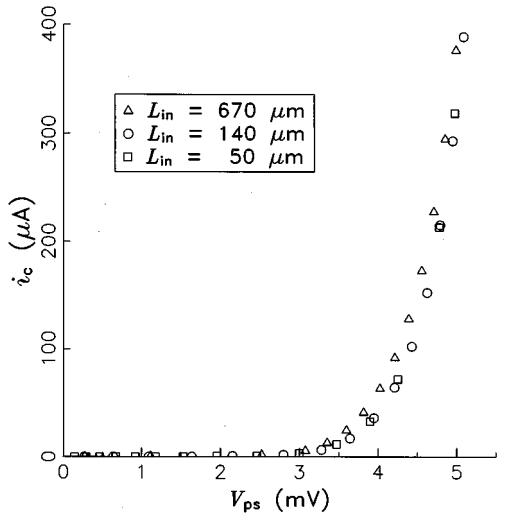

FIG. 17. Simulated i_c-V_{ps} relations for inner contact pair separations of 50, 140, and 670 μm, and other parameters as in Fig. 13.

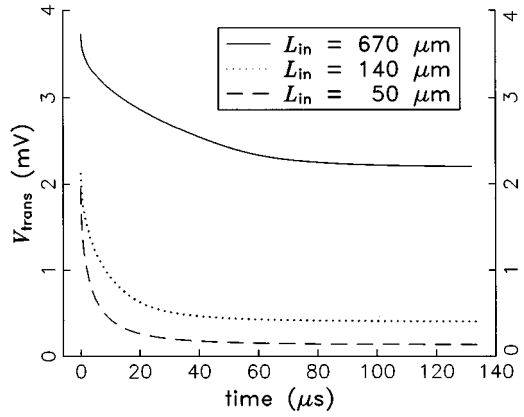

FIG. 18. Simulated transient voltage response to a current sign reversal in the transposed four-probe configuration, for inner contact pair separations of 50, 140, and 670 μm, and other parameters as in Fig. 13.

tact separation. Consequently, Ramakrishna *et al.* predicted that the prefactor I_0 in Eq. (4) should vary linearly with L_{in} and that V_{ps} for a given i_c should decrease with increasing L_{in}. In contrast, Maher *et al.* found no obvious variation of I_0 or $V_{ps}(i_c)$ for L_{in} varying by a factor of 100. Figure 17 compares i_c-V_{ps} relations obtained from simulations with L_{in}= 50, 140, and 670 μm. Both the i_c-V_{ps} relations and the I_0 values obtained by fitting them are independent of L_{in}, consistent with Maher *et al.*'s results.

B. X-ray measurements of CDW strain

Phase-slip-related strains $\epsilon \propto \partial\theta/\partial x$ produce local changes in the CDW wave vector $\Delta Q = \partial\theta/\partial x$ that can be directly measured using x-ray diffraction. DiCarlo *et al.*[17] measured the wave-vector shift in a 4.5 mm long $NbSe_3$ sample, and found that ΔQ varied approximately linearly with position in the middle two-thirds of the sample, consistent with the present results; the shift near the current contacts could not be measured because of geometrical constraints. Assuming that the CDW strain varied linearly with position over the entire length between current contacts, Ref. 17 estimated the CDW elastic constant K using Eq. (2) as

$$K = \left(\frac{en_c}{Q}\right)\left(\frac{V_{ps}}{L}\right)\left(\frac{\partial \Delta Q}{\partial x}\right)^{-1}, \tag{28}$$

where $\partial\Delta Q/\partial x$ is the x-ray-determined wave-vector gradient for a particular CDW current and V_{ps} is the phase-slip voltage for that current, estimated from the measurements of Ref. 15. The resulting value $K = 1.7\times10^{-2}$ eVÅ^{-1} is roughly a factor of 5 larger than estimated using mean-field theory.

This estimate must be modified, since the strain only varies linearly near the middle of the sample and is strongly enhanced near the current contacts. To a good approximation, the strain at the current contacts is proportional to V_{ps}. For a given V_{ps} and K, the midsample strain gradient will be smaller than if the profile was linear. Consequently, the assumption of a linear profile in Eq. (28) overestimates K, and makes the CDW appear stiffer than it is. Simulations using conditions comparable to those in the x-ray experiment suggest that K was overestimated by roughly a factor of 2, which is comparable to other uncertainties in the estimate in Ref. 17.

C. Transient response measurements

The transient CDW response to bipolar current pulses in $NbSe_3$ has been extensively studied using four-probe measurements. These measurements average over the spatial variations and can provide only limited information. In this section, we discuss what can and cannot be determined from four-probe measurements, and describe simulation results that provide insight into some puzzling previous observations.

1. Form of the four-probe response

Four-probe measurements of the transient response have generally been performed using the transposed configuration. For the T_{P_1} CDW in $NbSe_3$, these measurements show a simple monotonic time variation that has been fit using exponential or stretched-exponential forms. Figure 18 shows the four-probe transposed response for three different current contact separations, obtained from simulations using the model and parameters[53] of Sec. V. Spatial averaging in four-probe measurement converts the complex spatiotemporal response in Figs. 5 and 13 into the monotonic form observed in experiments. Contrary to suggestions in many previous analyses, this implies that the stretched-exponential time dependence used to fit four-probe transient response data has no fundamental significance. In particular, it does not reflect an intrinsic distribution of pinning strengths or metastable states, but results from a boundary-condition-related distribution of CDW strains.

2. Four-probe measurements and V_{ps}

Four-probe measurements cannot be used to determine the CDW strain profile, but they can provide some information about the magnitude of the strain. In particular, the initial and steady-state transposed voltages $V_{trans}(t=0^+)$ and

$V_{\rm trans}(t\rightarrow\infty)$ measured following a reversal of current direction are related to the phase-slip voltage $V_{\rm ps}$ defined in Sec. VI A.

The difference between the initial and steady-state voltages can be determined by combining Eq. (7) and Eq. (21). Noting that $\int_{-\infty}^{+\infty}(\partial^2\theta/\partial x^2)dx=0$ and $i_{\rm tot,norm}(t=0^+)=i_{\rm tot,norm}(t\rightarrow\infty)$ gives

$$V_{\rm trans}(t=0^+)-V_{\rm trans}(t\rightarrow\infty)$$
$$=\frac{\rho_s}{\rho_c+\rho_s}\left[-\int_{-\infty}^{+\infty}E_{P,\rm trans}(x,t=0^+)dx+\int_{-\infty}^{+\infty}E_{P,\ \rm trans}(x,t\rightarrow\infty)dx\right]. \quad (29)$$

As discussed in Sec. IV C, E_P is uniquely determined by i_c for $i_c(x,t)\neq 0$; for $i_c(x,t)=0$, E_P can take on a range of values and is determined by the CDW elastic force. Beyond the current contacts the profiles of both the CDW current and elastic force are symmetric about zero, giving $E_{P,\rm trans}(x,t=0^+)=-E_{P,\rm trans}(x,t\rightarrow\infty)$ in this region. Between the current contacts the CDW current i_c is nonzero and determines $E_P(x,t)$. In general, the initial and steady-state CDW current and elastic-force profiles must be used to determine the E_P profiles in Eq. (29). But if the initial and steady-state CDW currents between the current contacts are large enough to saturate the $E_P(i_c)$ variation in Fig. 7, the integrals between the current contacts in Eq. (29) will cancel, so that

$$V_{\rm trans}(t=0^+)-V_{\rm trans}(t\rightarrow\infty)$$
$$\approx\frac{\rho_s}{\rho_c+\rho_s}\left[-\int_{\rm out}E_{P,\rm trans}(x,t=0^+)dx+\int_{\rm out}E_{P,\rm trans}(x,t\rightarrow\infty)dx\right] \quad (30)$$
$$\approx\frac{\rho_s}{\rho_c+\rho_s}2V_{\rm ps}. \quad (31)$$

The simulated transposed four-probe responses in Fig. 18 used $\rho_s/(\rho_c+\rho_s)\approx 1/4.35$ and applied currents chosen to yield the same $V_{\rm ps}=3.3$ mV in each case. Equation (31) thus predicts that $V_{\rm trans}(t=0^+)-V_{\rm trans}(t\rightarrow\infty)\approx 1.5$ mV. This prediction is in good agreement with the simulation results for all three contact separations, even though the CDW currents $i_c\approx$ 50 μA are not large enough for full saturation of $E_P(i_c)$ in Fig. 7.

3. Measurements of CDW polarizations

Four-probe transient response measurements have been widely used to measure CDW polarizations. When the applied current direction is reversed, the CDW evolves from being compressed near one contact to being compressed near the other, and the CDW phase profile evolves between roughly parabolic profiles of opposite sign. The difference between the steady-state profiles defines a space-averaged phase displacement, corresponding to a net CDW polarization and charge flow.

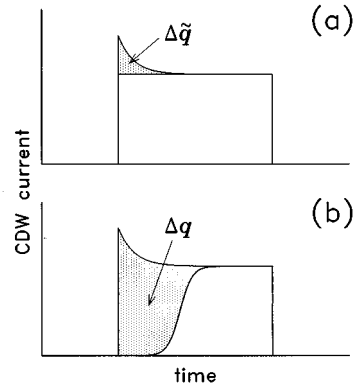

FIG. 19. Comparison of methods for determining the CDW polarization charge from the transient response. The shaded area in (a) indicates the charge $\Delta\tilde{q}$ of Eq. (32). The shaded area in (b) indicates the true polarization charge Δq. The lower curve in (b) indicates the phase-slip current corresponding to the total phase-slip rate $R_{\rm ps}(t)$ in Fig. 13. The polarization current is the difference between the total CDW current (upper curve) and the phase-slip current.

Previous analysis[9,31,32,40] of the CDW response to bipolar current pulses has assumed that this polarization charge is given by the transient *excess* charge flow,

$$\Delta\tilde{q}=\int_0^\infty[i_c(t)-i_c(t\rightarrow\infty)]dt. \quad (32)$$

This charge is indicated by the shaded region in Fig. 19(a). The results obtained using this assumption have been problematic, and inconsistent with theoretical expectations. The present analysis makes clear the reason for these difficulties: $\Delta\tilde{q}$ and the CDW polarization charge are not equivalent, because the total CDW current is a mix of polarization and phase-slip currents, and the polarization current is significantly larger than the transient excess during most of the transient.

In the steady state, the CDW phase profile and thus the CDW polarization are constant. The CDW polarization current is then zero (i.e., $\partial\theta/\partial t=0$) and the entire CDW current flow (determined by $\partial\phi/\partial t$) is due to phase slip. The estimate of the polarization charge in Eq. (32) assumes that the phase-slip current remains equal to its steady-state value throughout the transient. But as shown in Fig. 10, when the applied current direction is reversed, the strain near the current contacts abruptly drops below the magnitude necessary for appreciable slip to occur. The net slip rate thus drops to zero. Only once the phase profile has evolved so that the strains near the contacts are large enough does the slip rate again become appreciable, and this does not occur until well into the transient. The actual polarization current, indicated schematically in Fig. 19(b), is in general larger than the transient excess current in Fig. 19(a), and the polarization charge is larger than the transient charge calculated in Eq. (32). For example, in the simulation of Fig. 13, the CDW polarization between the current contacts is a factor of 10 larger than estimated using Eq. (32).

Since the polarization and phase-slip currents and their spatial variations cannot be independently measured, the net CDW polarization cannot be easily determined from tran-

sient response measurements. In principle, for applied voltages just above threshold, such that essentially no phase slip occurs, $\Delta\tilde{q}$ determined using Eq. (32) closely approximates the CDW polarization charge. In practice, just above threshold the transient is small and has a long time scale, particularly in longer samples, so that accurately subtracting the steady-state response to determine the excess current and charge is very difficult.

For applied currents well above threshold, a rough estimate of the net CDW polarization can be obtained by assuming that no phase slip occurs during the part of the transient, where $\Delta v \propto \Delta i_c$ is large. In particular, Eq. (32) is replaced with

$$\Delta\tilde{q} = \int_0^{t_0} i_c(t)dt, \tag{33}$$

where t_0 is a time where the transient response is mostly completed, e.g., the time for Δv to decay to $1/e$ of its initial value.

4. Length dependence of the transient response

Gill[9] has measured the charge $\Delta\tilde{q}$, for fixed V_{ps} in $NbSe_3$ at $T=90$ K, as a function of the current contact separation L_c. The measurements were performed near threshold, where the phase-slip rates are small, so that $\Delta\tilde{q}$ as given by Eq. (32) provides a reasonable estimate of the actual CDW polarization charge Δq. Gill found that $\Delta\tilde{q}$ is approximately independent of L_c for L_c between 100 and 1700 μm. This result was surprising because, for the strain profile of Eq. (2), the polarization charge should vary linearly with L_c.

The length independence of the polarization charge results because, as discussed in Sec. V C, most of the CDW phase displacement between the current contacts in samples shorter than $\sim$ 1000 μm is due to CDW deformations beyond the current contacts. In the transposed configuration used in Gill's experiments, the polarization current is given by $i_{pol}=A(en_c/Q)(1/L_c)\int_{-\infty}^{\infty}(\partial\theta/\partial t)dx$, defined in analogy to Eq. (22), where $i_{pol}\approx i_{c,trans}(t)-R_{ps}(t)$.[54] Integration of this current gives

$$\Delta q = \int_0^{\infty} i_{pol}(t)dt = A\left(\frac{en_c}{Q}\right)\left(\frac{1}{L_c}\right)\int_0^{+\infty}\int_{-\infty}^{+\infty}\partial\theta/\partial t\ dx\ dt \tag{34}$$

$$= A\left(\frac{en_c}{Q}\right)\left(\frac{1}{L_c}\right)\int_{-\infty}^{+\infty}[\theta(t\rightarrow\infty)-\theta(t=0)]dx$$

$$= A\left(\frac{en_c}{Q}\right)2\bar{\theta}. \tag{35}$$

Thus, the measured charge $\Delta\tilde{q}\approx\Delta q$ should be proportional to the space-averaged phase displacement $\bar{\theta}$.

Table I shows simulation results for $\bar{\theta}$ versus current contact separation L_c, assuming equal contact strains and thus approximately equal V_{ps} values. Because of CDW deformations beyond the current contacts, $\bar{\theta}$ and the polarization charge Δq vary by less than a factor of three for L_c between 50 and 3000 μm. An approximately linear variation of Δq with L_c is expected in longer samples, but measuring the transient response in conditions that do not produce phase slip in long samples is extremely difficult.

VII. DISCUSSION AND CONCLUSION

This paper has presented spatially resolved measurements of the CDW current profile and its temporal evolution. From these measurements the phase-slip, elastic force, and strain profiles and their temporal evolutions have been determined.

Fundamental to an understanding of this data is the coupling between the CDW current and elastic force implied by Eq. (7). This coupling arises because an applied current flows as CDW current and single-particle current. When the driving current and CDW current are both constant, the consequences of this coupling are trivial. But when the CDW current varies relative to the drive, the balance between CDW damping, pinning, and elastic forces must vary. In particular, when phase-slip results in a decrease in CDW current near the current contacts, the resulting decrease in the CDW damping force must be compensated by an increase in the elastic force. Small changes in CDW current can produce large changes in the elastic force: a 10% decrease in $i_c(x)$ can increase the elastic force by a factor of 3.

Strong evidence for this coupling is provided by the measured dc and transient CDW current profiles in Fig. 9, which are quantitatively related as predicted by Eq. (7). Perhaps more convincing is the close agreement between the measured and calculated spatiotemporal responses in Fig. 5 and Fig. 13. Here, the surprisingly complex experimental response is quantitatively reproduced using a single choice of the CDW elastic constant K as the only free parameter.

The consequences of the CDW current–elastic-force coupling are significant: the transient response magnitude near the current contacts is enhanced; the steady-state CDW strain and phase-slip rates near the current contacts are enhanced; and the length scale on which significant phase slip occurs is reduced. The coupling also affects interpretation of previous measurements of phase slip in $NbSe_3$. As previously assumed, the CDW strain at the current contacts is approximately proportional to the phase-slip voltage V_{ps} determined from four-probe measurements, although deviations become appreciable at large CDW currents. Because of the strain and slip-rate enhancements near the current contacts, the i_c-V_{ps} relations should be roughly independent of current contact separation, consistent with the measurements reported in Ref. 15.

Aside from confirming the CDW current–elastic-force coupling, the agreement between the measured spatiotemporal response in Fig. 5 and the predictions in Fig. 13 provide additional evidence for the importance of phase slip in CDW dynamics. Phase slip limits the strain which can be developed near the current contacts, and introduces interesting structure into the transient response, e.g., the dip and recovery seen for segments ± 4 in Fig. 5. The good qualitative agreement between the measured and simulated transient responses in Fig. 5 and Fig. 13 does not necessarily validate the specific slip-strain relation Eq. (3) used in the simulation, but is likely a general consequence of including phase slip.

Information about the phase-slip mechanism is provided by the phase-slip distribution and the local slip-rate–strain relations, determined from the measured CDW current and

strain profiles. Phase slip is highly localized near the current contacts; in Fig. 4, 90% of the phase slip occurs within 30 μm of the current contacts. This is a consequence of strain enhancements arising from the CDW current–elastic-force coupling, and is consistent with a slip rate that is driven by and varies rapidly with strain, such as described by Eq. (3).

Much of the previous work on phase slip has assumed that the local slip rate is a function only of the local strain. The local slip–strain relation measured near the current contacts, where most of the phase slip occurs, is qualitatively consistent with Eq. (3) predicted for slip by homogeneous thermal nucleation of dislocation loops, and is quantitatively consistent with the i_c-$V_{\rm ps}$ relations determined in four-probe measurements. This suggests that the total phase-slip rate is dominated by local phase slip as described by Eq. (3), and that slip is dislocation-generation limited. However, some phase slip occurs at distances of hundreds of micrometers from the current contacts, where CDW strains are small. For a given strain, the slip rates in this region are much larger than near the current contacts. This implies that the local slip rate depends upon parameters other than the local strain.

This is not surprising. Phase slip involves at least two steps: the formation of a CDW dislocation loop or line, which requires a minimum CDW strain; and the growth and motion of these defects, so as to remove a CDW phase front in the entire crystal cross section, which requires much smaller strains.[3,7,9,25,55] The analysis that leads to Eq. (3) only calculates the defect formation rate.[14] But as discussed by Gill,[25,55] dislocations may persist for a considerable time and may drift or glide considerable distances from where they are formed, producing phase slip there. Thus, the phase-slip process should be nonlocal. Near the current contacts where the strains are largest, dislocation formation may dominate the slip rate; away from the contacts, the strains are too small to form new dislocations, so growth of dislocations formed elsewhere may dominate.

An upper bound on the longitudinal dislocation velocity can be obtained from the spatially resolved transient response measurements of Fig. 5. Segments ± 2 attain their steady-state CDW current, and hence their steady-state phase-slip rate, within 80 μs. Assuming that slip in these segments is due to dislocations formed at the current contacts 195 μm away, the dislocation velocity must be at least 240 cm/s. The CDW velocity in Fig. 5 is only 5 cm/s, roughly 50 times smaller. This suggests that the dislocations must move through rather that with the CDW, perhaps by glide rather than drift. Similar differences between CDW and dislocation velocities have been reported previously.[56] Dislocation dynamics may also play a role in producing the curious initial rise in Fig. 5 for segments near the middle of the sample.

CDW deformations beyond the current contacts play a surprisingly important role in transient CDW dynamics. These deformations are responsible for most of the mid-sample phase displacement observed for current contact separations of less than 1 mm, and strongly affect the magnitude and time scale of the transient response. Although deformations beyond the contacts may be large, the phase-slip rates there are very small. This is indicated by the large transient but small steady-state currents/voltages seen for segments ± 5 in both the measured and simulated responses of Figs. 5 and 13.

Finally, although the results and analysis presented here have focused on the T_{P_1} CDW in $NbSe_3$, they should be readily generalized to describe CDW's in other materials. CDW formation in $NbSe_3$ (as well polytypes of TaS_3 and NbS_3) leaves part of the Fermi surface ungapped, so that the single-particle density is large at all temperatures. The single-particle resistance R_s is essentially independent of the CDW's state of deformation, allowing the single-particle and CDW currents to be unambiguously separated and greatly simplifying analysis. In fully gapped semiconducting CDW materials such as $K_{0.3}MoO_3$, the single-particle density freezes out with decreasing temperature, and CDW deformations can change the single-particle resistance by several percent. This deformation-resistance coupling should modify some details of the CDW response, particularly near threshold where the CDW current–elastic-force coupling has little effect. But the basic physics described here should still dominate. This suggestion is supported by recent spatially resolved optical transmission measurements of CDW deformations in $K_{0.3}MoO_3$,[47] which show generally similar behavior to that described here.

In conclusion, we have performed spatially resolved measurements of the CDW response to bipolar current pulses, and have shown that these measurements directly yield the distribution of CDW phase slip and the temporal evolution of the CDW elastic-force and strain profiles. We have demonstrated that the CDW elastic-force profile is strongly coupled to the phase-slip distribution, and have used a simple model that includes this coupling to account for many features of the observed response. These results demonstrate the importance of knowing the full profile of CDW motion between and beyond the current contacts in understanding CDW dynamics.

ACKNOWLEDGMENTS

We wish to acknowledge fruitful conversations with J. C. Gill, J. W. Brill, V. Ambegaokar, C. Myers, and P. Monceau. Sample substrates were fabricated at the National Nanofabrication Facility at Cornell University. This work was supported by NSF Grant Nos. DMR92-04169 and DMR94-24572.

*Permanent address: Institute of Radioengineering and Electronics, Russian Academy of Sciences, Moscow, Russia.

[1] For comprehensive reviews of CDW's, see P. Monceau, *Electronic Properties of Quasi-One-Dimensional Materials* (Reidel, Dordrecht, 1985), Pt. II, p. 139; G. Grüner, Rev. Mod. Phys. **60**, 1129 (1988).

[2] H. Fukuyama and P. A. Lee, Phys. Rev. B **17**, 535 (1978).

[3] P. A. Lee and T. M. Rice, Phys. Rev. B **19**, 3970 (1979).

[4] L. Sneddon, M. Cross, and D. Fisher, Phys. Rev. Lett. **49**, 292 (1982); H. Matsukawa and H. Takayama, J. Phys. Soc. Jpn. **56**, 1507 (1987); H. Matsukawa, *ibid.* **56**, 1522 (1987); **57**, 3463 (1988); S. N. Coppersmith and P. B. Littlewood, Phys. Rev. B **36**, 311 (1987); A. Middleton and D. Fisher, *ibid.* **47**, 3530 (1993).

[5] N. P. Ong, G. Verma, and K. Maki, Phys. Rev. Lett. **52**, 663 (1984); N. P. Ong and K. Maki, Phys. Rev. B **32**, 6582 (1985).
[6] L. P. Gor'kov, Pis'ma Zh. Éksp. Teor. Fiz. **38**, 76 (1993) [JETP Lett. **38**, 87 (1983)].
[7] D. Feinberg and J. Friedel, in *Low-Dimensional Electronic Properties of Molybdenum Bronzes and Oxides*, edited by C. Schlenker (Kluwer, Dordrecht, 1989), p. 407.
[8] J. C. Gill, Solid State Commun. **44**, 1041 (1982).
[9] J. C. Gill, J. Phys. C **19**, 6589 (1986); Physica **143B**, 49 (1986).
[10] K. Maki, Physica **143B**, 59 (1986).
[11] P. Monceau, M. Renard, J. Richard, and M. C. Saint-Lager, Physica **143B**, 64 (1986).
[12] D. V. Borodin, S. V. Zaitsev-Zotov, and F. Ya. Nad', Zh. Éksp. Teor. Fiz. **93**, 1394 (1987) [Sov. Phys. JETP **66**, 793 (1987)].
[13] For a comprehensive review of previous work on CDW phase slip, see F. Ya. Nad', in *Charge Density Waves in Solids*, edited by L. P. Gor'kov and G. Grüner (Elsevier, New York, 1989), p. 189.
[14] S. Ramakrishna, M. P. Maher, V. Ambegaokar, and U. Eckern, Phys. Rev. Lett. **68**, 2066 (1992); S. Ramakrishna, Phys. Rev. B **48**, 5025 (1993).
[15] M. P. Maher, T. L. Adelman, S. Ramakrishna, J. P. McCarten, D. A. DiCarlo, and R. E. Thorne, Phys. Rev. Lett. **68**, 3084 (1992).
[16] L. Mihaly and A. Janossy, Phys. Rev. B **30**, 3530 (1984); S. E. Brown, L. Mihaly, and G. Grüner, Solid State Commun. **58**, 231 (1986).
[17] D. DiCarlo, E. Sweetland, M. Sutton, J. D. Brock, and R. E. Thorne, Phys. Rev. Lett. **70**, 845 (1993).
[18] V. Ya. Pokrovskii and S. V. Zaitsev-Zotov, Synth. Met. **29**, F439 (1989).
[19] S. V. Zaitsev-Zotov, Solid State Commun. **76**, 17 (1990).
[20] M. P. Maher, T. L. Adelman, J. McCarten, D. A. DiCarlo, and R. E. Thorne, Phys. Rev. B **43**, 9968 (1991).
[21] S. N. Coppersmith, Phys. Rev. Lett. **65**, 1044 (1990).
[22] T. L. Adelman, M. C. de Lind van Wijngaarden, S. V. Zaitsev-Zotov, D. DiCarlo, and R. E. Thorne, Phys. Rev. B **52**, R5483 (1995).
[23] T. L. Adelman, Ph.D. thesis, Cornell University, 1995.
[24] M. P. Maher, T. L. Adelman, D. A. DiCarlo, J. P. McCarten, and R. E. Thorne, Phys. Rev. B **52**, 13 850 (1995).
[25] J. C. Gill, in *Physics and Chemistry of Inorganic Conductors*, edited by C. Schlenker and M. Greenblatt (Plenum, New York, in press).
[26] M. E. Itkis and J. W. Brill, Phys. Rev. Lett. **72**, 2049 (1994).
[27] M. C. Saint-Lager, P. Monceau, and M. Renard, Synth. Met. **29**, F279 (1989).
[28] J. C. Gill, Solid State Commun. **39**, 1203 (1981).
[29] R. M. Fleming, Solid State Commun. **43**, 167 (1982).
[30] G. Mihaly and L. Mihaly, Solid State Commun. **48**, 449 (1983); G. Mihaly, G. Kriza, and A. Janossy, Phys. Rev. B **30**, 3578 (1984).
[31] Z. Z. Wang and N. P. Ong, Phys. Rev. Lett. **58**, 2375 (1987).
[32] J. Zhang, J. F. Ma, S. E. Nagler, and S. E. Brown, Phys. Rev. Lett. **70**, 3095 (1993).
[33] J. Dumas and A. Arbaoui, J. Phys. (France) IV **3**, C2-179 (1993).
[34] E. Sweetland, A. C. Finnefrock, W. J. Podulka, M. Sutton, J. D. Brock, D. DiCarlo, and R. E. Thorne, Phys. Rev. B **50**, 8157 (1994).
[35] R. E. Thorne, Phys. Rev. B **45**, 5804 (1992). Also, see, F. Levy and H. Berger, J. Cryst. Growth **61**, 61 (1983).
[36] The polymer film was formed by placing the sample onto the patterned substrate and applying a drop of ethyl cellulose dilutely dissolved in methanol. Subsequent evaporation of the methanol left an approximately 0.2 μm film holding the sample to the substrate.
[37] The measured steady-state voltage for segments ± 5 (20 μm beyond the current contacts) is less than 30 μV. Due to contributions from electric field fringing near the current contacts, the small voltage observed cannot be attributed to CDW conduction in this region.
[38] M. C. de Lind van Wijngaarden *et al.* (unpublished).
[39] J. C. Gill, Phys. Rev. Lett. **70**, 331 (1993).
[40] M. E. Itkis and S. V. Zaitsev-Zotov, J. Phys. (France) IV **3**, C2-193 (1993).
[41] F. Ya. Nad', M. E. Itkis, P. Monceau, and M. Renard, J. Phys. France IV **3**, C2-175 (1993).
[42] The first 0.5 μs of the transient response was not recorded. The value of $i_c(t=0)$ was estimated by extrapolating the measured values to $t=0$.
[43] Evidence for static CDW deformations beyond current contacts is discussed in Ref. 27.
[44] At fields above a few times threshold, E_P is directly related to perturbative corrections to the dc CDW conductivity from its Ohmic high-field limit calculated in Refs. 4.
[45] From the data of Fig. 6, the maximum i_c variation is 80 μA which, from Fig. 7, corresponds to a 15 mV/cm variation in E_P. From Eq. (7), this E_P variation modifies the CDW current by about 4.5 μA, or about 5% of the i_c variation. Therefore, most of the i_c transient is due to the transient elastic force.
[46] The CDW current profile in Fig. 4 is slightly asymmetric and depends upon the current direction, so that the strain in the middle of the sample is likely to deviate slightly from zero.
[47] M. E. Itkis, B. M. Emerling, and J. W. Brill, Phys. Rev. B **52**, R11 545 (1995).
[48] In this estimate, the offset ϵ_0 was chosen so that the strains at the two current contacts are the same.
[49] The simulation used $\rho_s = 7.76\times10^4\ \Omega\ \mathrm{m}^{-1}$, $\rho_c = 2.60\times10^5\ \Omega\ \mathrm{m}^{-1}$, $V_a = 31$ mV, $r_0 = 5\times10^{15}\ \mathrm{s}^{-1}\ \mathrm{m}^{-1}$, $K = 6.21\times10^{-3}$ eV Å^{-1}, $en_c/Q = 4.33\times10^{-3}\ e\ \text{Å}^{-2}$, and the experimentally determined $E_P(i_c)$ relation for this sample.
[50] The estimate of DiCarlo *et al.*, $K = 1.7\times10^{-2}$ eV Å^{-1}, assumed a linear strain profile. As discussed in Sec. VI B, use of the actual strain profile should reduce the value of K by roughly a factor of two.
[51] For example, the time scale of E_P's response to a current direction reversal may be slower at 90 K than at 120 K.
[52] This approximation neglects the small asymmetry in the current profile, which produces an asymmetry in the strain profile.
[53] The simulation assumes that the outer contact pair separation is much larger than the inner contact pair separation.
[54] Taking the CDW displacement current as $i_{c,\mathrm{trans}}(t) - R_{\mathrm{ps}}(t)$ assumes that all of the phase-slip occurs at the current contacts. To exactly separate the polarization current from the phase-slip current, it is necessary to know not only the total phase-slip rate, but its spatial dependence.
[55] J. C. Gill, J. Phys. France IV **3** C2-3, 165 (1993).
[56] J. C. Gill, Europhys. Lett. **11**, 175 (1990).